Electronic Supplementary Material (ESI) for CrystEngComm

Supporting Information

of

Investigation on a New Organic/Inorganic Hybrid Crystal Tri(p-chloro-anilium) Pentabromocadmate (II) by In-situ PXRD and FTIR Methods: Thermal Stability and the Route to Suppress its Decomposition

Lili Cao,[a] Zhi Liu,*[a] Tao Wang,[a] Hongxia Dai,[a] Liangmin Zhang,[b] Xutang Tao[a] and Deliang Cui[a]
a State Key Laboratory of Crystal Materials, Shandong University, Jinan 250100, P. R. China
b Arkansas Center for Laser Applications and Science, Department of Chemistry and Physics, Arkansas State University, P. O. Box 419, AR 72467, USA

S1 Supplementary materials for crystal structure

Crystallographic data have been deposited in the Cambridge Crystallographic Data Center, CCDC No. 693833. Copies of these data may be obtained from the director, CCDC, 12 Union Road, Cambridge CB2 1EZ, UK. Tel.: +44-1223-762910; Fax: +44-1223-336033; e-mail: deposit@ccdc.cam.ac.uk or on the web http://www.ccdc.cam.ac.uk/ deposit.

For depicting the spatial arrangement of organic and inorganic components in $(p\text{-Cl-}C_6H_4NH_3)_3CdBr_5$, an asymmetric unit of this hybrid crystal is presented in Fig. S1. Each asymmetric unit consists of three $p\text{-Cl-}C_6H_4NH_3$ ligands and one $CdBr_5^{3-}$ anion.

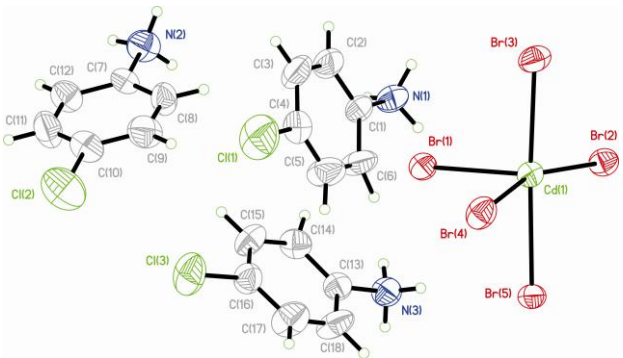

Fig. S1 Perspective view of the asymmetric unit of the hybrid crystal, showing the atom-numbering scheme, displacement ellipsoids are drawn at the 50% probability level.

S2 Two modes used in the in-situ FTIR monitoring experiments

In the in-situ FTIR monitoring experiments, both the transmission modes and diffusive reflectance were applied, and their schematic diagrams are presented in Fig. S2. The transmission mode is very sensitive to the gaseous products released by the hybrid crystal when being heated (Fig. S2 (a)), thus this mode was used to continuously detect the gaseous products when heating the hybrid crystal at different temperatures. On comparison, for detecting the changes of the hybrid crystal, the diffusive reflectance mode is an appropriate and quite sensitive tool (Fig. S2 (b)).

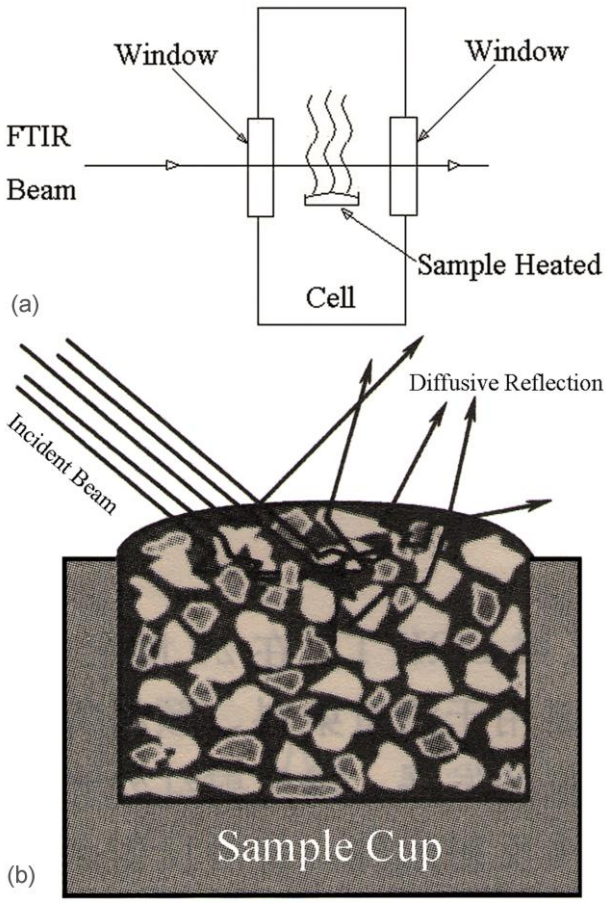

Fig. S2 Schematic diagrams of the transmission mode (a) and diffusive reflectance mode (b) applied in in-situ FTIR experiments.

S3 Verifying the uniformity of the sample by using powder X-ray diffraction pattern

The powder XRD pattern was usually used to examine if there are impurity phases in a sample. In Fig. S3, the powder XRD pattern of our sample as well as the calculated pattern of monoclinic $(p\text{-Cl-}C_6H_4\text{-}NH_3)_3CdBr_5$ are presented. By comparing the measured XRD pattern with the calculated one, it was found that they matched with each other quite well, revealing that the sample comprises pure monoclinic $(p\text{-Cl-}C_6H_4\text{-}NH_3)_3CdBr_5$.

Electronic Supplementary Material (ESI) for CrystEngComm

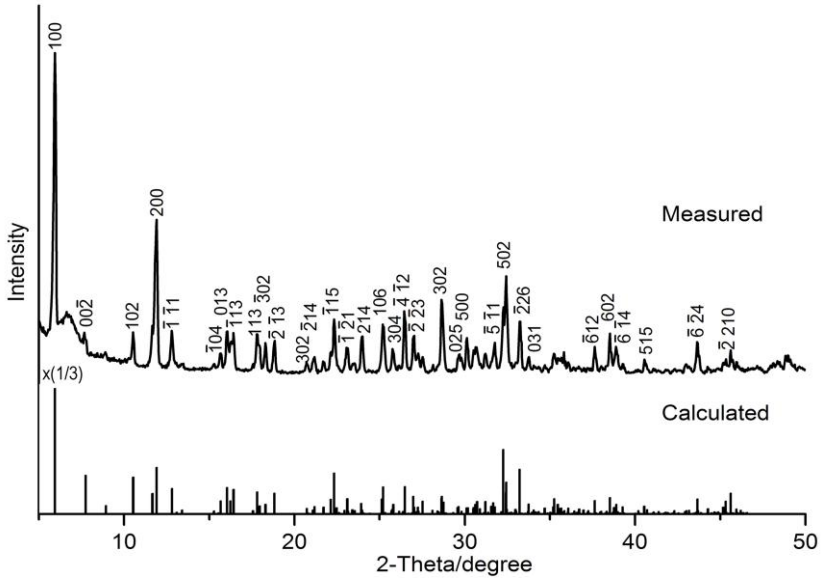

Fig. S3 Powder XRD patterns of the hybrid crystal (p-Cl-C_6H_4-NH_3)$_3CdBr_5$. Top: measured XRD pattern, bottom: calculated XRD pattern of monoclinic (p-Cl-C_6H_4-NH_3)$_3CdBr_5$.

S4 Identifying the remaining product obtained after TGA measurement of the hybrid crystal

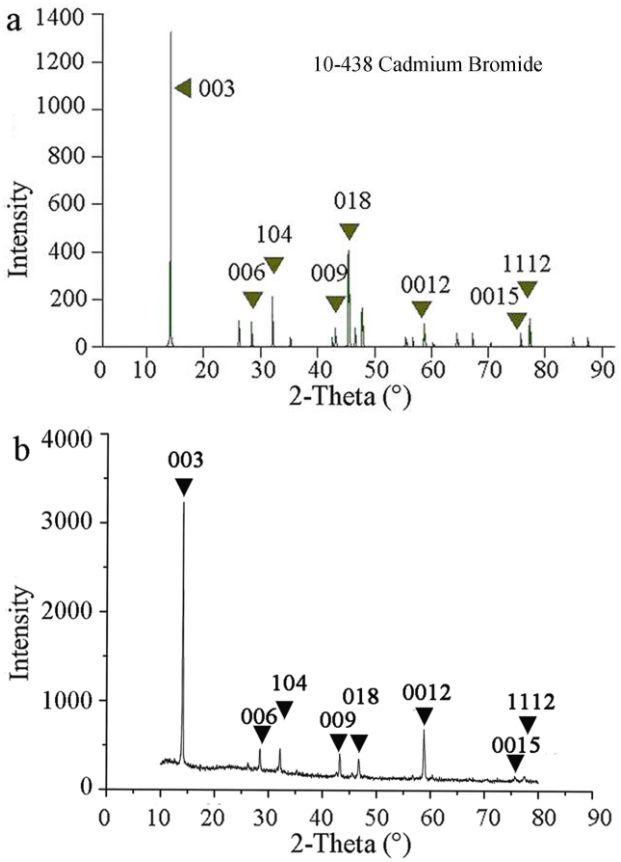

Fig. S4 (a) Standard XRD pattern of R-$CdBr_2$, (b) XRD pattern of the remanent solid obtained by heating (p-C_6H_4-NH_3)$_3CdBr_5$ at 250 ˚C for 2 h.

After heating the hybrid crystal (p-Cl-C_6H_4-NH_2)$_3CdBr_5$ at 250 ˚C in nitrogen for 2 h, the remaining solid product was collected for XRD characterization, and the result was presented in Fig. S4. For making comparison, the standard XRD pattern of R-$CdBr_2$ was also presented in Fig. S4. By comparing the two patterns, it is clear that the remaining solid is R-$CdBr_2$.

S5 Detailed information of the p-Cl-C_6H_4-NH_2HBr crystal

According to the proposed thermal decomposition processes in the manuscript, the p-Cl-C_6H_4-NH_2HBr crystal was synthesised to identify the two diffraction peaks appeared (2θ=6.2 ˚ and 12.6 ˚) in the in-situ XRD measurement at 170 ˚C.

Crystals of p-Cl-C_6H_4-NH_2HBr were prepared as follows: To a solution of p-Cl-C_6H_4-NH_2 (3.6 g, 28.2 mmol) in 15 ml of ethanol, 9 ml of concentrated aqueous HBr (40%) was added in drop-wise way for ten minutes under an atmosphere of Ar. The reaction mixture was stirred at room temperature for 1 hour. The product p-Cl-C_6H_4-NH_2HBr was isolated as colorless crystals (4.2 g, 72.1%) by solvent evaporation method from above solution. The diffraction data of single crystal were collected at 293(2) K using a Bruker P4 diffractometer (Mo Kα radiation, λ = 0.71073 Å). Cell parameters were retrieved using SMART software and then refined using SAINTPlus software. The crystal crystallizes in monoclinic space group $P2_1/c$ with unit cell parameters a = 4.4980(6) Å, b = 6.1858(8) Å, c = 14.4538(18) Å, α = 90.9386(17)˚, β = 94.9448(17)˚, γ = 100.0386(13)˚, V = 394.33(9) Å^3, Z = 2, $R_1[F^2 > 2\sigma(F^2)]$ = 0.0741, wR_2 = 0.1572. Its crystallographic data have been deposited in the Cambridge Crystallographic Data Center, CCDC No. 844699. Copies of these data may be obtained from the director, CCDC, 12 Union Road, Cambridge CB2 1EZ, UK. Tel.: +44-1223-762910; Fax: +44-1223-336033; e-mail: deposit@ccdc.cam.ac.uk or on the web http://www.ccdc.cam.ac.uk/ deposit.

The powder XRD pattern of p-Cl-C_6H_4-NH_2HBr, with the diffraction faces being indentified according to the calculated X-ray diffractogram in Fig. S5 (a), was collected at room temperature. The diffraction angles of (001) and (002) peaks

locate at 2θ=6.1 ˚ and 12.3 ˚ respectively. In another word, the two peaks emerged from 170 ˚C in Fig. 3 exactly derived from *p*-Cl-C_6H_4-NH_2HBr (their intensity are too weak at 170 ˚C, so the pattern achieved at 185 ˚C was plotted in Fig. S5 (b)).

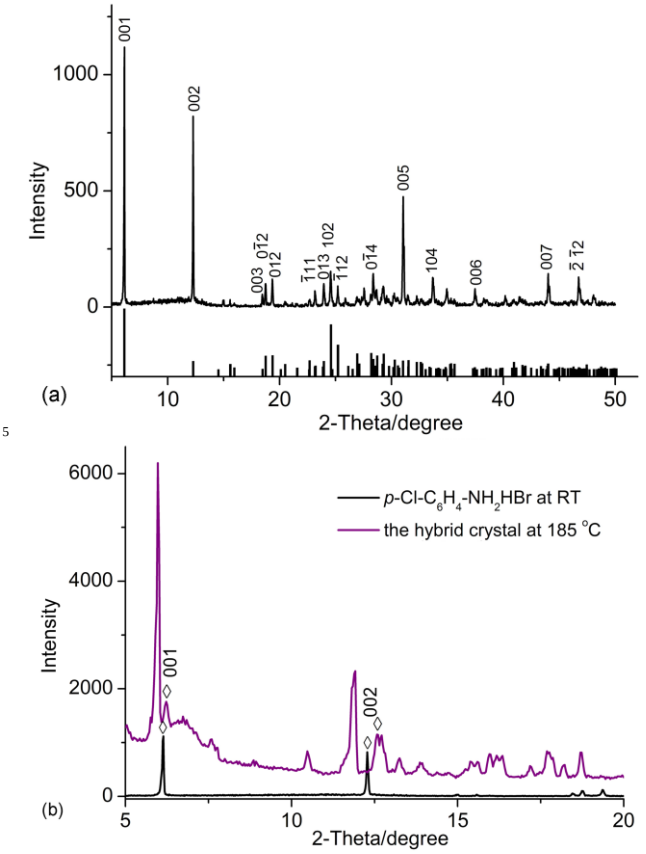

Fig. S5 (a) Identification of Powder XRD patterns of *p*-Cl-C_6H_4-NH_2HBr. Top: measured powder XRD pattern, bottom: the calculated one. (b)The two peaks appeared when the (*p*-Cl-C_6H_4-NH_3)$_3CdBr_5$ crystal was heated to 185 ˚C coincide well with (001) and (002) diffraction peaks of *p*-Cl-C_6H_4-NH_2HBr.

The thermal stability was determined using TGA-DSC measurements using a SDT Q600 V8.0 Build 95 thermal analyzer. As shown in Fig. S6, the extension starting decomposition temperature is determined at about 180˚C. The endothermic peak at 125 ˚C come from water or solvent absorbed on the testing sample. The one endothermic peak at 184 ˚C on DSC curve demonstrates the moment when the crystal structure starts to dissociate. It overlies on the broad strong one at 225 ˚C, which is attributed to the subsequent fast decomposition process of the crystal.

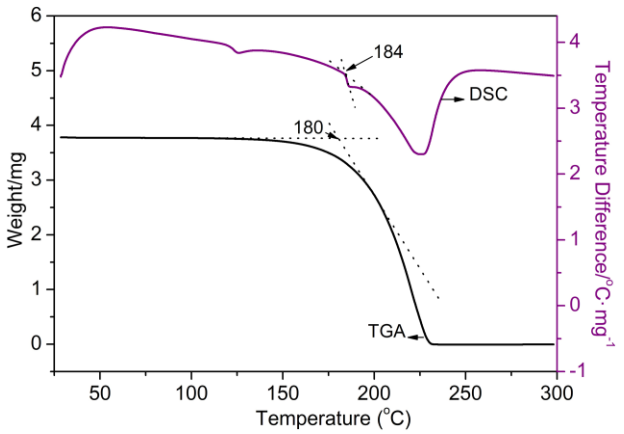

Fig. S6 TGA-DSC curves of p-Cl-C_6H_4-NH_2HBr crystal. The endothermic peaks toward downward. The curves are obtained in 100 ml/min N_2 flow. The scanning speeds are: 25-150 ˚C, 10 ˚C/min; 150-300 ˚C, 5 ˚C/min.

S6 Red-shift of the absorption peak of - NH_3^+ when the hybrid crystal dissociated

From the infrared absorption spectrum of the *p*-Cl-C_6H_4-NH_2HBr crystal, it is found that the peak corresponding to the symmetric and asymmetric stretching vibration modes of $-NH_3^+$ located at ~2890 cm^{-1} as the little chart inserted in Fig. S7 (a). On comparison, this peak is at ~3040 cm^{-1} in the hybrid crystal. The experimental results reveal that, when the hybrid crystal was heated to 170 ˚C, this characteristic absorption peak started to red-shifted remarkably from 3040 cm^{-1} to 2890 cm^{-1} (as shown in Fig. S7). It means that *p*-Cl-C_6H_4-NH_2HBr emerged in the crucible used in the diffusive reflectance mode. Correspondingly, the weight of the hybrid crystal decreased rapidly, and the peak at 2645 cm^{-1} disappeared at 170 ˚C. These results confirm again that the peak at 2645 cm^{-1} can be used as the "finger-print" of the hybrid crystal in the in-situ monitoring experiments.

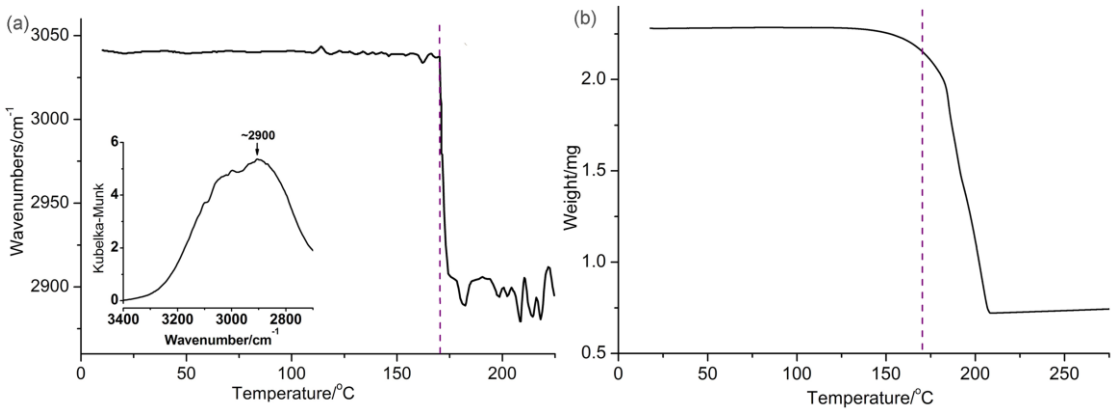

Fig. S7 (a) Red-shift of the peak of $-NH_3^+$ when heating the hybrid crystal (*p*-Cl-C_6H_4-NH_3)$_3CdBr_5$ (a little chart was inserted to exhibit $-NH_3^+$ stretching vibration of *p*-Cl-C_6H_4-NH_2HBr), (b) TGA curve of the hybrid crystal is also presented for comparison.